88
Review paper
Doi 10.61892/STP202601013B
ISSN 2566-4484

Miloš Basarić, Military Geographical Institute, mbasaricbp@gmail.com
Dušan Jovanović, University of Novi Sad, dusanbuk@uns.ac.rs

# IDENTIFICATION OF GEOMETRIC DISTORTIONS IN SENTINEL-1 IMAGERY OVER THE TERRITORY OF SERBIA CAUSED BY THE SLANT OBSERVATION GEOMETRY OF SAR SYSTEMS

***Abstract:***

This study systematically identifies and analyzes geometric distortions, specifically layover and shadow effects, in Sentinel-1 imagery across the Republic of Serbia. The research quantifies these distortions caused by slant observation geometry. The primary contribution is a unique, publicly available spatial dataset representing distortion distribution for both ascending and descending orbits at a national scale. The analysis evaluates the magnitude of these effects across diverse topographic profiles, establishing a quantitative benchmark for assessing Sentinel-1 data usability.

*Keywords: Sentinel-1, SAR, Geometric distortions, Radar shadow, Layover.*

# ИДЕНТИФИКАЦИЈА ГЕОМЕТРИЈСКИХ ДИСТОРЗИЈА НА SENTINEL-1 СНИМЦИМА НА ТЕРИТОРИЈИ СРБИЈЕ ИЗАЗВАНИХ КОСОМ ГЕОМЕТРИЈОМ ОСМАТРАЊА SAR СИСТЕМА

***Сажетак:***

Ова студија систематски идентификује и анализира геометријске дисторзије, специфично ефекте преклапања (*layover*) и радарске сјенке, на *Sentinel-1* снимцима на територији Републике Србије. Истраживање квантификује ове дисторзије узроковане косом геометријом осматрања. Примарни допринос је јединствен, јавно доступан просторни скуп података који представља дистрибуцију дисторзија за узлазну и силазну орбиту на националном нивоу. Анализа процјењује учесталост ових ефеката кроз различите топографске профиле, успостављајући квантитативно мјерило за оцјену употребљивости Sentinel-1 података.

*Кључне ријечи: Sentinel-1, SAR, геометријска дисторзија, радарска сенка, преклапање.*

# 1. INTRODUCTION

Synthetic Aperture Radar (SAR) systems represent an important source of satellite imagery for observing the Earth's surface, owing to their ability to operate independently of illumination and weather conditions. However, due to their side-looking imaging geometry, SAR data are affected by geometric distortions that arise from applying a two-dimensional imaging system to a three-dimensional, topographically complex surface, under the implicit assumption that the terrain is flat and devoid of elevation variations [1], [2]. These distortions lead to systematic errors in radar signal projection, particularly in areas of pronounced relief. We cannot effectively use backscattered signals from these areas to understand ground properties [3], from an InSAR perspective, these distortions destroy the continuity of interferometric phase images and pose significant challenges for subsequent phase unwrapping [4], [5]. Therefore, the identification and spatial delineation of areas prone to geometric limitations in SAR imaging is of particular importance, since these regions are required to be excluded from any further analysis [2]. In the context of SAR imaging geometry, the term SAR distortions primarily refer to layover and shadow effects, while foreshortening, although also a geometric distortion, can be largely mitigated during image processing and is therefore generally considered less critical for most analytical applications [6].

Various methods for detecting areas affected by layover and shadow have been proposed over the past three decades. Some approaches are based on the direct derivation of these phenomena using sensor platform geometry and digital elevation models (DEM) [7], [8], while others rely on purely GIS-based analyses performed prior to radar data acquisition [9]. Additional methods focus on detecting these areas using multi-angle or co-registered SAR acquisitions [4], [10]. In several studies, machine learning techniques have been applied for the identification of distortion-affected areas [11], [12], [13]. Furthermore, Li et al. proposed an image fusion approach based on SAR scenes acquired under different geometric configurations to compensate for areas affected by geometric distortions, thereby reducing error rates and improving the usability of SAR products [14].

Numerous studies have addressed the identification of distortion-affected zones using data from various spaceborne and airborne SAR platforms. There are multiple motivations for mapping such areas, ranging from accurate radiometric analysis aimed at quantifying information loss caused by signal overlaps, to quality control of geocoded SAR products, where distortion maps serve as reference layers for identifying spatial positioning errors [7]. In addition, such datasets are essential for determining the measurable displacement fraction of potential landslides [9] and for other InSAR-based application use cases [15], [16].

The main objective of this study is the systematic identification and spatial analysis of geometric distortions, primarily layover and shadow effects, in Sentinel-1 SAR imagery covering the territory of the Republic of Serbia. Although these phenomena are well understood in theory and have been extensively investigated in previous studies, their spatial distribution at the national scale has not yet been comprehensively analyzed within the regional context.

The primary scientific contribution of this research lies in the creation of a unique spatial dataset that quantitatively and cartographically represents the distribution of geometric distortions in Sentinel-1 radar imagery across Serbia. This dataset enables a systematic assessment of the spatial variability of radar distortions and provides a foundation for further studies in interferometry, ground deformation monitoring, and the optimization of reference object placement, such as corner reflectors. The Sentinel-1 mission represents one of the key contemporary implementations of SAR technology, whose open data policy enables extensive scientific and operational applications, including long-term time series analyses and the development of national and regional ground motion monitoring services [17]. In this context, understanding the spatial distribution of geometric distortions constitutes a fundamental prerequisite for the correct interpretation of radar products and for improving the reliability of derived results.

In this way, the present study contributes to the advancement of methodological approaches in national and regional SAR data analysis and provides a reference framework for future applications of Sentinel-1 data in geoscientific and engineering studies in Serbia and the wider region. The generated spatial dataset is publicly available and open-access, ensuring methodological transparency, reproducibility of results, and the potential for reuse in future research.

## 2. THEORETICAL BACKGROUND OF SAR GEOMETRY

Unlike optical systems, which rely on the intensity of reflected solar energy and central perspective, SAR systems operate based on measuring the return time of the transmitted microwave pulse [7]. The acquisition geometry is side-looking, which is necessary to avoid signal ambiguity that would arise from echoes arriving simultaneously from both the left and right sides of the sensor relative to nadir.

As a consequence of their side-looking geometry, synthetic aperture radar systems generate images with a number of unusual image features, which are often readily apparent when observing a radar image [1].

### 2.1. ACQUISITION GEOMETRY

A SAR sensor operates by transmitting radar pulses and recording the time, frequency, and phase of the backscattered signal. Typical off-nadir/side-looking viewing angles ($\gamma$) range between 15° and 60° [2], as illustrated in Figure 1. For easier interpretation, SAR data are commonly converted into ground-range geometry by projecting distances onto a horizontal reference surface. However, this transformation assumes smooth terrain and therefore introduces geometric distortions in areas with significant topographic relief, since elevated terrain is physically closer to the sensor than its projection onto the local geoid [1], [2]. An important parameter in SAR imaging geometry is the incidence angle ($\eta$), defined as the angle between the incoming radar beam and the surface normal at the point of illumination. In Figure 1, $H$ represents the height at which the sensor is located, while $\theta v$ is vertical beamwitdth. This angle strongly influences both the magnitude of the backscattered signal and the severity of geometric distortions. Steeper viewing angles tend to increase layover effects, whereas shallower viewing angles are more likely to produce radar shadow [1].

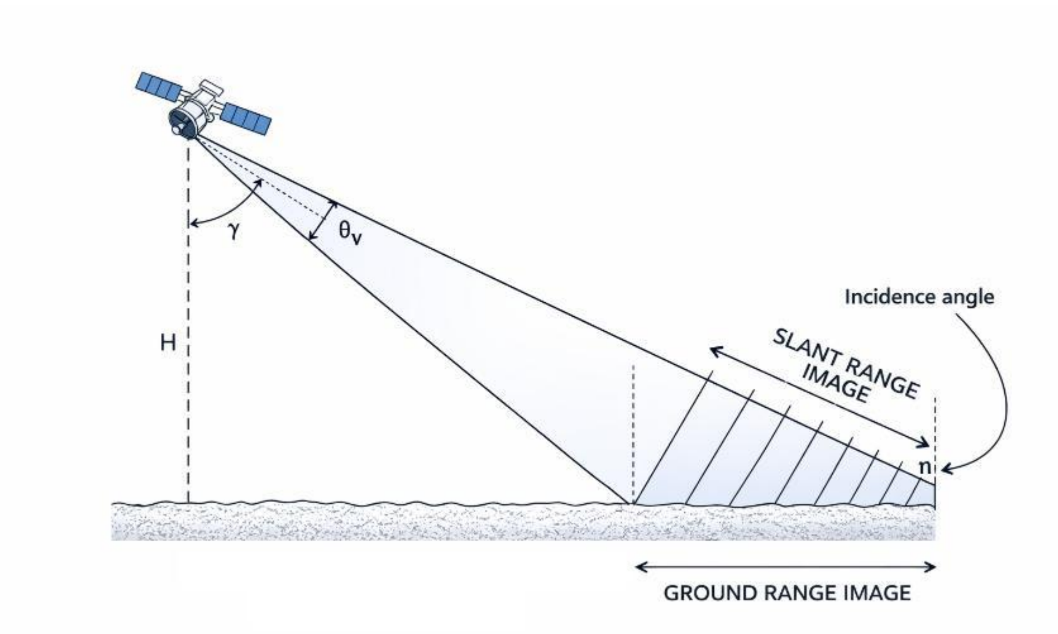


*Figure 1. Representation of SAR side looking geometry [3].*

Without terrain correction, this displacement can lead to significant geometric misinterpretation of SAR imagery over rugged areas [1]. When a digital elevation model (DEM) is available, these terrain-induced distortions can be corrected through orthorectification, resulting in geometrically accurate SAR image products [2]. In addition to terrain displacement, the side-looking geometry causes the formation of layover and shadow regions. Since the backscattered signal from these areas cannot be reliably related to surface properties, corresponding masks must be generated to exclude them from further analysis [2].

### 2.2. GEOMETRIC DISTORTIONS: LAYOVER AND SHADOW

Radar shadow is the most intuitive distortion among the aforementioned phenomena and is closely related to everyday experience, as well as to the fundamental understanding of electromagnetic radiation. In cases where the back-slope angle $\alpha$ exceeds the SAR side-looking angle $\gamma$, the terrain geometry prevents the radar pulse from reaching the slope. This occlusion occurs because higher topographic features block the signal, resulting in a radar shadow. Consequently, regions such as *S* in Figure 2 fail to return any backscatter, appearing as dark patches dominated by thermal or speckle noise [4]. Shadow regions will occur on any terrain where the back-slope angle exceeds $\pi/2 - \eta$ [2].

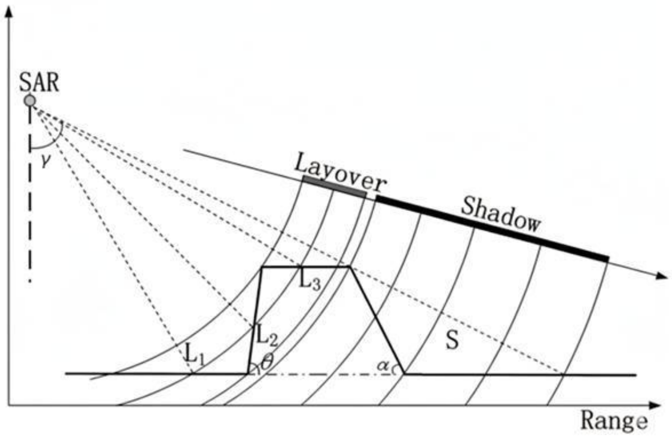


*Figure 2. Illustration of SAR Layover and Shadow Phenomena [4].*

Layover is generated when the fore-slope angle $\theta$ exceeds the SAR side-looking angle $\gamma$, which results in the radar echo from the top of the slope reaching the SAR receiver earlier than the echo from the slope base. Since the sensor-to-target distances for these points (L1, L2, and L3) are equal, the corresponding backscattered signals are projected onto the same image pixel [4], as shown in Figure 2. As a result, the superposition of these signals produces layover effects that are observed as bright areas in SAR images with no practical method of separating the contributions from different points on the ground [2].

### 2.3. ORBITAL INFLUENCE

The accuracy of identifying geometric distortions, such as layover and shadow zones, directly depends on the precision of satellite position knowledge at the time of acquisition. During the radar imaging process, any deviation in the orbital trajectory leads to an incorrect interpretation of signal travel time, which manifests as a geometric offset in the final product. As reported in [18], a strict orbital accuracy requirement of 5 cm in 3D has been defined for the Sentinel-1 mission, which is necessary to meet the scientific objectives of the mission. In order to correctly align the digital terrain model (DTM) with the radar imagery, it is essential to use Precise Orbit Determination (POD) data, since even minimal variations in the satellite center-of-mass position or antenna offset can affect geolocation accuracy.

In the context of Serbia's terrain, where mountainous regions such as Kopaonik or Tara are prone to pronounced distortions, the use of precise orbital data is critical. Previous studies have shown that modeling inaccuracies, such as variations in the antenna phase center, directly influence radial orbit errors, which may lead to systematic biases in sensor position interpretation [19]. Without the application of these corrections, areas affected by radar shadow or layover would be spatially misaligned with the actual terrain conditions. Such geometric offsets would degrade the reliability of analyses over Serbian territory, as distortion masks would be projected with positional shifts relative to the digital terrain model, thereby preventing accurate spatial analysis and data fusion with other geospatial datasets.

## 3. MATERIALS AND METHODOLOGY

### 3.1. DATA

#### 3.1.1. Study area

The territory of the Republic of Serbia was selected as the study area (AOI) for the identification of geometric distortions in SAR imagery. Data describing the national boundary of Serbia were obtained in shapefile (.shp) format from the open-access DIVA-GIS portal [20]. The selection of Serbia as the area of interest was not motivated solely by its geographical extent, but by the need to establish a unified spatial dataset that can serve as a prerequisite for future SAR-related research and provide scientific validation of SAR "usable zones" at the national level. The national boundary dataset was further used as a spatial search criterion during the searching and downloading of SAR imagery.

### 3.1.2. Sentinel-1 imagery

The data were obtained from the Alaska Satellite Facility (ASF) Data Search platform (Vertex) [21]. Sentinel-1 scenes covering the territory of Serbia were downloaded in Level-1 Single Look Complex (SLC) format, acquired in Interferometric Wide Swath (IW) mode under both ascending (satellite flight path from south to north) and descending (satellite flight path from north to south) orbit geometries [22]. Layover and radar shadow effects are inherent to the slant-range geometry of SAR systems and can only be reliably identified using Single Look Complex (SLC) data, which preserves the original radar acquisition geometry. In contrast, Ground Range Detected (GRD) products undergo radiometric and geometric transformations that alter the original imaging geometry, making them unsuitable for precise detection of terrain-induced geometric distortions. Both ascending and descending Sentinel-1 acquisitions were therefore used to derive geometric distortion masks, as SAR layover and radar shadow effects strongly depend on the sensor viewing geometry. Terrain slopes that are favorably imaged in one orbit direction may be severely affected by geometric distortions in the opposite viewing geometry. The combined use of ascending and descending datasets ensures a comprehensive identification of distortion-prone areas and reduces the risk of underestimating terrain-induced SAR imaging limitations. Ascending and descending Sentinel-1 SLC scenes were selected within the same short temporal window (22–25 November) to ensure temporal consistency during the computation of geometric distortion masks. Since layover and shadow distortions are primarily determined by sensor acquisition geometry and the underlying DEM, their spatial patterns remain essentially stable over time for a given Sentinel-1 geometry. The selected short temporal window ensures consistency and facilitates standardized processing, but using acquisitions from other dates would yield nearly identical distortion masks, with only minimal differences. A total of 13 ascending acquisitions were collected along relative orbits 73 (absolute orbit 5144), 175 (absolute orbit 62022), 102 (absolute orbit 5173) and 29 (absolute orbit 62051). Scenes from relative orbits 73 and 102 were acquired by the Sentinel-1C satellite, while scenes from relative orbits 175 and 29 were acquired by Sentinel-1A. In addition, 13 descending acquisitions were collected along relative orbits 51 (absolute orbit 5122), 153 (absolute orbit 62000), 80 (absolute orbit 5151), and 7 (absolute orbit 62029). Scenes from relative orbits 153 and 7 were acquired by Sentinel-1A, whereas scenes from relative orbits 51 and 80 were acquired by Sentinel-1C. An overview of the acquired ascending scenes is provided in Table 1, while the descending acquisitions are summarized in Table 2.

The proposed methodology is valid under the current Sentinel-1 orbital configuration and imaging geometry, which has been operationally stable since Sentinel-1 mission started. If future missions introduce different acquisition geometries, the methodology remains transferable by adapting new geometry parameters.

*Table 1. Technical characteristics and metadata of the Ascending SAR imagery dataset.*

**Ascending**

| | Path | Frame | Date | Satellite | Absolute Orbit | Layover | Shadow | Combined (L&S) |
|---|---|---|---|---|---|---|---|---|
| 1 | 73 | 148 | 23.11.2025. | Sentinel-1C | 5144 | Yes | — | — |
| 2 | 73 | 143 | 23.11.2025. | Sentinel-1C | 5144 | — | — | — |
| 3 | 73 | 138 | 23.11.2025. | Sentinel-1C | 5144 | Yes | Yes | Yes |
| 4 | 175 | 132 | 24.11.2025. | Sentinel-1A | 62022 | Yes | Yes | Yes |
| 5 | 175 | 137 | 24.11.2025. | Sentinel-1A | 62022 | Yes | Yes | Yes |
| 6 | 175 | 142 | 24.11.2025. | Sentinel-1A | 62022 | Yes | Yes | Yes |
| 7 | 175 | 147 | 24.11.2025. | Sentinel-1A | 62022 | — | — | — |
| 8 | 102 | 134 | 25.11.2025. | Sentinel-1C | 5173 | Yes | Yes | — |
| 9 | 102 | 139 | 25.11.2025. | Sentinel-1C | 5173 | Yes | — | — |
| 10 | 102 | 145 | 25.11.2025. | Sentinel-1C | 5173 | — | — | — |
| 11 | 102 | 150 | 25.11.2025. | Sentinel-1C | 5173 | Yes | Yes | — |
| 12 | 29 | 138 | 26.11.2025. | Sentinel-1A | 62051 | — | — | — |
| 13 | 29 | 143 | 26.11.2025. | Sentinel-1A | 62051 | Yes | Yes | — |

*Table 2. Technical characteristics and metadata of the Descending SAR imagery dataset.*

**Descending**

| | Path | Frame | Date | Satellite | Absolute Orbit | Layover | Shadow | Combined (L&S) |
|---|---|---|---|---|---|---|---|---|
| 1 | 51 | 438 | 22.11.2025. | Sentinel-1C | 5122 | — | — | — |
| 2 | 51 | 443 | 22.11.2025. | Sentinel-1C | 5122 | Yes | Yes | — |
| 3 | 51 | 448 | 22.11.2025. | Sentinel-1C | 5122 | Yes | Yes | — |
| 4 | 153 | 438 | 23.11.2025. | Sentinel-1A | 62000 | Yes | — | — |
| 5 | 153 | 443 | 23.11.2025. | Sentinel-1A | 62000 | Yes | Yes | — |
| 6 | 153 | 448 | 23.11.2025. | Sentinel-1A | 62000 | Yes | Yes | Yes |
| 7 | 153 | 453 | 23.11.2025. | Sentinel-1A | 62000 | Yes | Yes | — |
| 8 | 80 | 440 | 24.11.2025. | Sentinel-1C | 5151 | Yes | Yes | Yes |
| 9 | 80 | 445 | 24.11.2025. | Sentinel-1C | 5151 | Yes | Yes | — |
| 10 | 80 | 450 | 24.11.2025. | Sentinel-1C | 5151 | Yes | Yes | — |
| 11 | 80 | 455 | 24.11.2025. | Sentinel-1C | 5151 | Yes | Yes | Yes |
| 12 | 7 | 448 | 25.11.2025. | Sentinel-1A | 62029 | Yes | Yes | — |
| 13 | 7 | 453 | 25.11.2025. | Sentinel-1A | 62029 | Yes | Yes | — |

Figure 3 presents the spatial footprints of the ascending (left, blue) and descending (right, red) Sentinel-1 imagery used in this study.

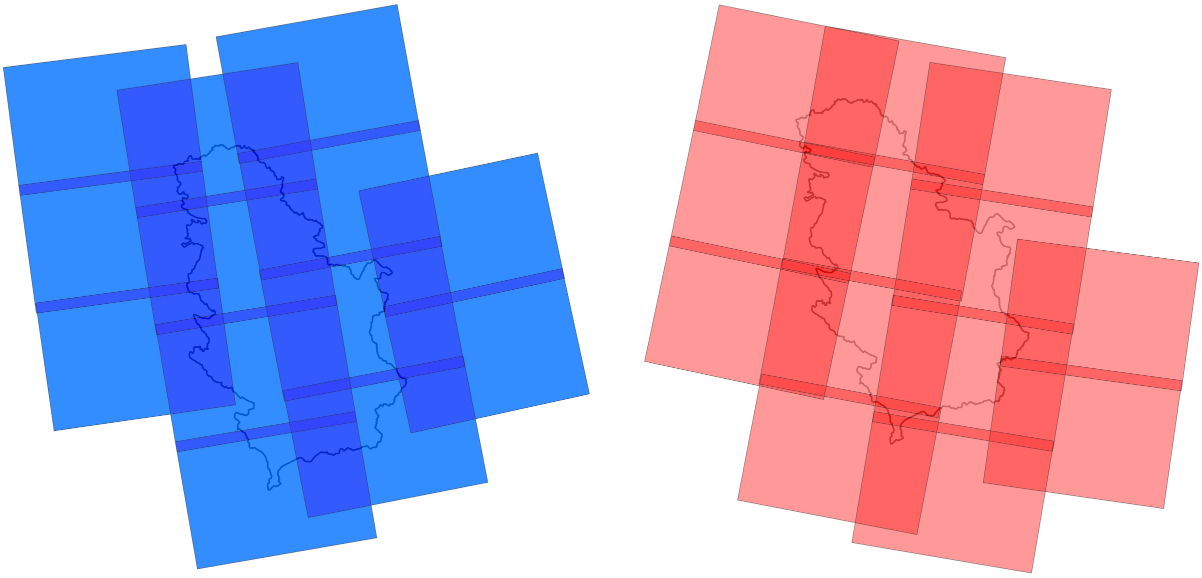

*Figure 3. Sentinel 1 imagery footprints (created by author).*

### 3.1.3. DIGITAL ELEVATION MODEL (DEM)

As the required digital elevation model for generating geometric distortion masks on the acquired Sentinel-1 SLC imagery, the SRTM 1 arc-second (HGT) digital elevation model, with an approximate spatial resolution of 30 m, was used [23], [24]. This DEM was selected as the default and baseline option within the SNAP software environment, where it represents a standard, readily available data source for SAR geometry–based analyses. The SRTM DEM is automatically downloaded and integrated into the processing workflow, ensuring a consistent and reproducible use of terrain information during the computation of layover and radar shadow masks.

## 3.2. METHODOLOGY

In order to identify and analyze geometric distortions in SAR imagery, a comprehensive data processing chain was defined and implemented (the processing workflow is illustrated in Figure 4). The processing chain consists of two main components. The first component involves SAR data processing in the ESA SNAP software environment [25], resulting in the generation of initial geometric distortion masks. The second component focuses on additional GIS-based processing using ArcGIS Pro [26] and the derivation of the final spatial dataset.

### 3.2.1. DISTORTION MASK GENERATION

The first processing step involved the application of precise orbit data using the Apply Orbit File operator, where Precise Orbit Ephemerides (POD) were used for all SAR scenes in order to improve geolocation accuracy. This was followed by the deburst procedure, which merges individual bursts into continuous images within each sub-swath. In the subsequent stage, SAR simulation and terrain correction were performed using the SAR Simulation and Terrain Correction operators [27], [28]. For this purpose, the Shuttle Radar Topography Mission digital elevation model in the SRTM 1 arc-second (HGT) format was automatically downloaded and integrated as the reference elevation dataset. Upon completion of this processing stage, distortion masks representing the spatial distribution of geometric distortions were generated based on 2-pass method, including layover masks, shadow masks, as well as combined layover-and-shadow masks for pixels affected simultaneously by both effects [29]. The 2-pass algorithm for detecting layover and shadow in SAR images processes the DEM twice. In the first pass, it moves from the sensor toward the far range, calculating the slant range to each terrain point; areas where the distance stops increasing and multiple signals overlap indicate layover, while changes in the illumination angle reveal shadows. In the second pass, it goes in the opposite direction, from far range to near range, to capture layover zones not fully detected in the first pass. The results of both passes are then combined to produce a complete layover and shadow map, enabling accurate interpretation and geocoding of SAR data [30]. The distortion masks were generated after terrain correction, ensuring that the final products were georeferenced in ground range geometry. The resulting distortion masks were finally exported in GeoTIFF format with an approximate spatial resolution of 10 m per pixel. All output masks were stored in the geographic coordinate reference system WGS 1984 (EPSG:4326), ensuring compatibility with standard GIS workflows and further spatial analyses.

### 3.2.2. GIS POST-PROCESSING

Due to the large spatial coverage and high spatial resolution characteristic of the IW acquisition mode, the resulting raster products and distortion masks exhibited very large file sizes and required substantial memory resources. Since the distortion masks are inherently binary in nature, a binary raster conversion procedure was applied in the subsequent processing step. This optimization significantly reduced file sizes and improved computational efficiency during further data processing. The optimized raster masks were then converted into vector format in order to enable advanced spatial manipulation and analysis. Within the vector processing stage, masks corresponding to ascending orbits were merged into a single vector layer, while masks derived from descending orbits were combined into a separate vector dataset. An overlap analysis was subsequently performed, taking into account the partial spatial overlap between individual SAR scenes. This procedure enabled the identification of locations where geometric distortions occur repeatedly, either within the same orbital configuration or across different orbit geometries, which was of particular analytical relevance.

As a result of the overlap analysis, distortion values were assigned according to the number of overlapping occurrences: locations with no mutual overlap were assigned a value of 1, areas with one overlap resulting from two intersecting scenes were assigned a value of 2, and locations affected by three overlapping scenes were assigned a value of 3.Following the completion of vector-based processing, the merged ascending and descending vector layers were converted back into raster format, preserving the categorical values 1, 2, and 3 corresponding to the degree of spatial overlap. The generated rasters were subsequently clipped to the area of interest defined by the administrative boundary of the Republic of Serbia, resulting in the final dataset used for further spatial analysis.

In order to further enhance the spatial robustness of the results and to mitigate potential effects of minor orbital geometry variations and uncertainties, two additional versions of the final raster datasets were generated using an expand operation. The masks were expanded by 2 and 5 pixels, respectively, producing one original and two expanded raster datasets.

The structure of the final dataset[1] consists of six raster layers:

- layover in ascending orbit geometry,
- layover in descending orbit geometry,
- shadow in ascending orbit geometry,
- shadow in descending orbit geometry,

[1] https://github.com/milosbassa/radar_distorsion_masks

- combined layover and shadow in ascending orbit geometry,
- combined layover and shadow in descending orbit geometry.

### 3.2.3. STATISTICAL AND SPATIAL ANALYSIS

To assess the spatial distribution and intensity of radar imaging distortions, a regular fishnet grid was generated over the study area and clipped by AOI. The grid consisted of 40 × 40 cells, with each cell covering an area of approximately 8 km × 12 km. This resolution was chosen after testing multiple grid sizes, as it provided the best balance between spatial detail and statistical stability. This spatial framework was used to normalize the analysis scale and enable consistent comparison of distortion patterns across the entire territory of Serbia. The input dataset consisted of a raster layer containing classified distortion values (1, 2, and 3). Zonal statistics were applied using the fishnet grid as zonal units, allowing raster-based distortion information to be aggregated into raster grid spatial summaries. This approach facilitates both quantitative analysis and cartographic visualization

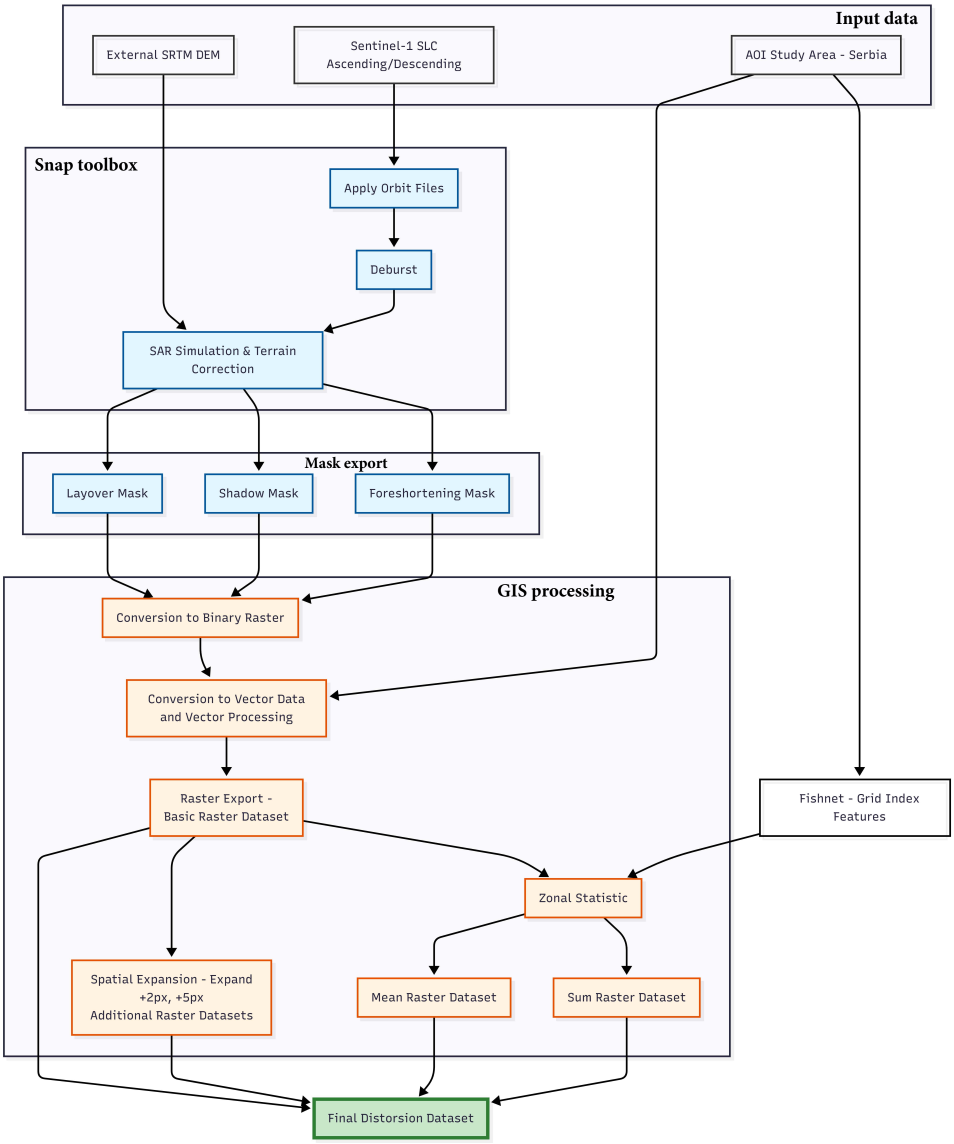


*Figure 4. Schematic representation of the data processing chain from Sentinel-1 SLC to distortion dataset (created by author).*

Two complementary statistical metrics were computed for each grid cell: *sum* and *mean*. The sum statistic was used to quantify the cumulative distortion intensity within each spatial unit. By aggregating all distortion pixel values inside a grid cell, these metric captures both the spatial extent of distortions and the effect of overlapping distortion occurrences. Areas characterized by repeated or spatially clustered distortions therefore yield higher sum values, effectively highlighting zones of persistent radar imaging degradation. This cumulative representation serves as a proxy for identifying spatial hotspots of distortion activity. In parallel, the mean statistic was calculated to estimate the average distortion intensity and spatial distribution within each grid cell. Unlike the sum metric, which emphasizes accumulation and spatial overlap, the mean value reflects the overall severity level of distortions normalized by the number of contributing pixels. This enables the identification of areas where distortions are consistently strong, even if their spatial extent is limited. The mean-based aggregation therefore provides insight into the local intensity structure of distortion patterns independent of areal coverage [31], [32].

The resulting zonal statistics layers were visualized using graduated color symbology in order to enhance interpretability and highlight spatial trends. This cartographic representation significantly improves the readability of the dataset and enables effective communication of large-scale distortion patterns, which would be difficult to interpret directly from the original raster products.

## 4. RESULTS AND DISCUSSION

Figure 5 presents a representative sample of the distortion mask generation workflow for the descending radar shadow case, displayed as a four-panel collage arranged in a strip-like reading order (from left to right in the upper row, followed by left to right in the lower row). The upper-left panel shows the local terrain morphology based on SRTM (World Hillshade) [33], while the upper-right panel illustrates the original distortion mask. In this mask, darker red pixel values indicate shadow areas that spatially overlap with shadow occurrences detected in other SAR acquisitions, whereas brighter red pixels represent isolated distortion instances specific to the analyzed scene geometry. The lower-left and lower-right panels display the expanded versions of the same mask expanded with 2 and 5 pixels, respectively. This progressive morphological expansion increases the spatial footprint of shadow-affected zones and incorporates boundary uncertainties related to sensor geometry and terrain-induced displacement effects.

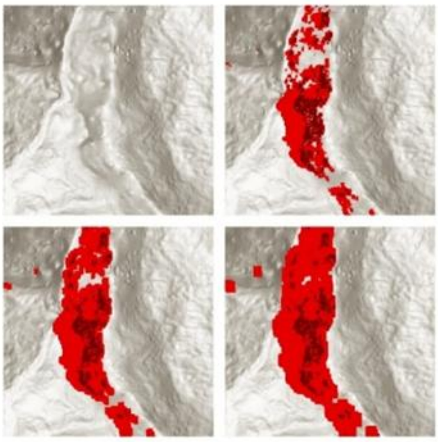

*Figure 5. Sample of descending radar shadow mask generation and pixel-based spatial expansion in mountainous terrain (created by author).*

The presented example is located within the Jerma Special Nature Reserve near Dimitrovgrad, eastern Serbia, and corresponds to a mountain slope with elevations reaching approximately 1300 m above sea level. The dominant shadow patterns are observed on the western-facing slope of the mountain terrain, which is consistent with the imaging geometry of descending acquisitions. This site was selected as a representative terrain-controlled distortion case and serves as an illustrative sample of the distortion mask characteristics.

### 4.1. STATISTICAL AND SPATIAL ANALYSIS OF DISTORTIONS

Figure 6 is organized into six panels illustrating the spatial distribution of mean-based zonal statistics for radar distortion types. The upper row corresponds to the ascending acquisition geometry, while the lower row represents the descending geometry. Within each row, the first panel depicts layover-related distortions, the second panel shows shadow effects, and the third panel illustrates areas affected by combined layover and shadow distortions. The same panel arrangement and visualization structure are applied in Figure 7, which presents the corresponding results derived using the sum-based statistical metric.

The mean-based zonal statistics (Figure 6) reveal distinct spatial patterns of radar distortions across Serbia, reflecting clear differences between ascending and descending acquisition geometries. For ascending acquisitions, layover and shadow effects are generally widespread. Layover distortions appear throughout the territory, with higher intensity clusters in western and central Serbia and a notable belt along the transition from central to southern Serbia extending eastward. Shadow distortions are similarly extensive, with minimal occurrences in central Serbia and Vojvodina, but dominant patterns in western and southern Serbia. Combined layover–shadow distortions in the ascending orbit are largely confined to localized areas, primarily in western Serbia.

In contrast, descending acquisitions exhibit considerably more constrained distortion patterns. Layover effects are mostly concentrated in the southern half of Serbia, including central Serbia, southern Kosovo and Metohija, and the Homolje regions, while shadow and combined distortions are minimal, with only minor occurrences along narrow linear zones, e.g., near Stara Planina. These observations suggest several key insights: first, distortion intensity and spatial distribution are strongly orbit-dependent, with ascending geometries producing more extensive and dispersed distortion patterns across the country. Second, western and central Serbia appear particularly susceptible to both layover and shadow effects, likely reflecting the interaction of terrain topography with radar incidence angles. Third, descending geometries produce fewer distortions overall, with the highest concentrations limited to specific southern regions. Finally, combined layover–shadow distortions are relatively rare, indicating that most distortions occur independently rather than overlapping extensively. Collectively, these results highlight the importance of considering acquisition geometry and regional terrain characteristics when interpreting SAR-derived products or planning interferometric analyses.

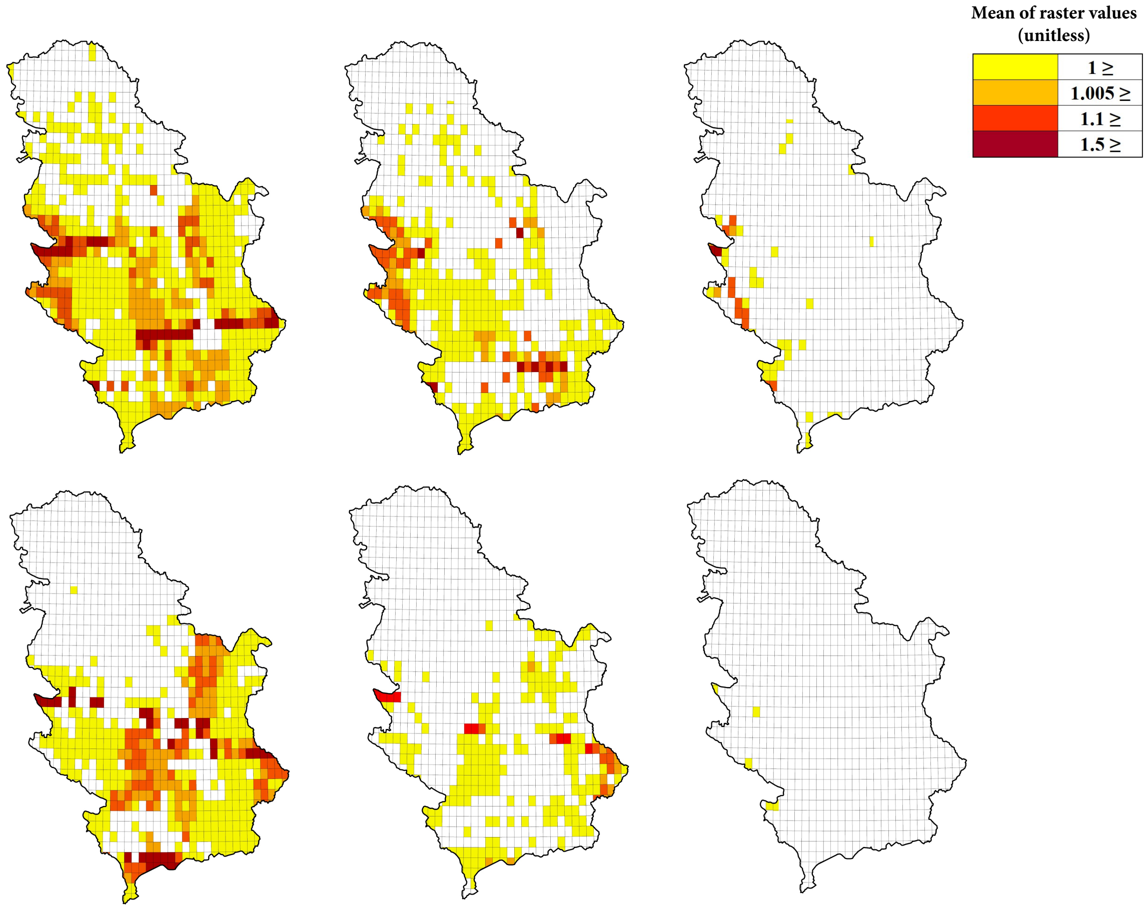


*Figure 6. Mean-based zonal statistics of radar distortions across Serbia (ascending: a–c layover, shadow, combined; descending: d–f layover, shadow, combined) (created by author)..*

The mean-based results emphasize the spatial distribution of average distortion severity. Several grid cells exhibit elevated mean values despite moderate cumulative coverage, indicating localized zones of consistently high distortion intensity. This highlights areas where even limited spatial extents of distortion may significantly affect data quality.

The sum-based zonal statistics presented in Figure 7 largely corroborate the patterns observed in the mean-based analysis (Figure 6), while providing additional insights into the cumulative intensity and overlap of radar distortions. For ascending acquisitions, layover distortions are again widespread across Serbia, similar to the mean-based results, but with stronger emphasis on central and eastern regions, including the southern and western parts of Kosovo and Metohija. This highlights areas with repeated distortion occurrences across multiple acquisitions, reflecting regions of persistent geometric interference. Shadow distortions under ascending geometry remain relatively minor and scattered, with sporadic overlap primarily in western Serbia, while combined layover–shadow distortions show similar spatial distribution to the mean-based statistics, concentrated in the west.

In descending acquisitions, layover distortions exhibit notable overlap across multiple scenes, particularly in southern and central Serbia, indicating higher cumulative distortion intensity than observed in the mean-based maps. Shadow effects remain limited and largely consistent with the mean-based observations, with minimal combined layover–shadow occurrences. Overall, descending distortions are more localized and less pervasive, reinforcing the earlier conclusion that acquisition geometry significantly influences both the extent and intensity of radar distortions.

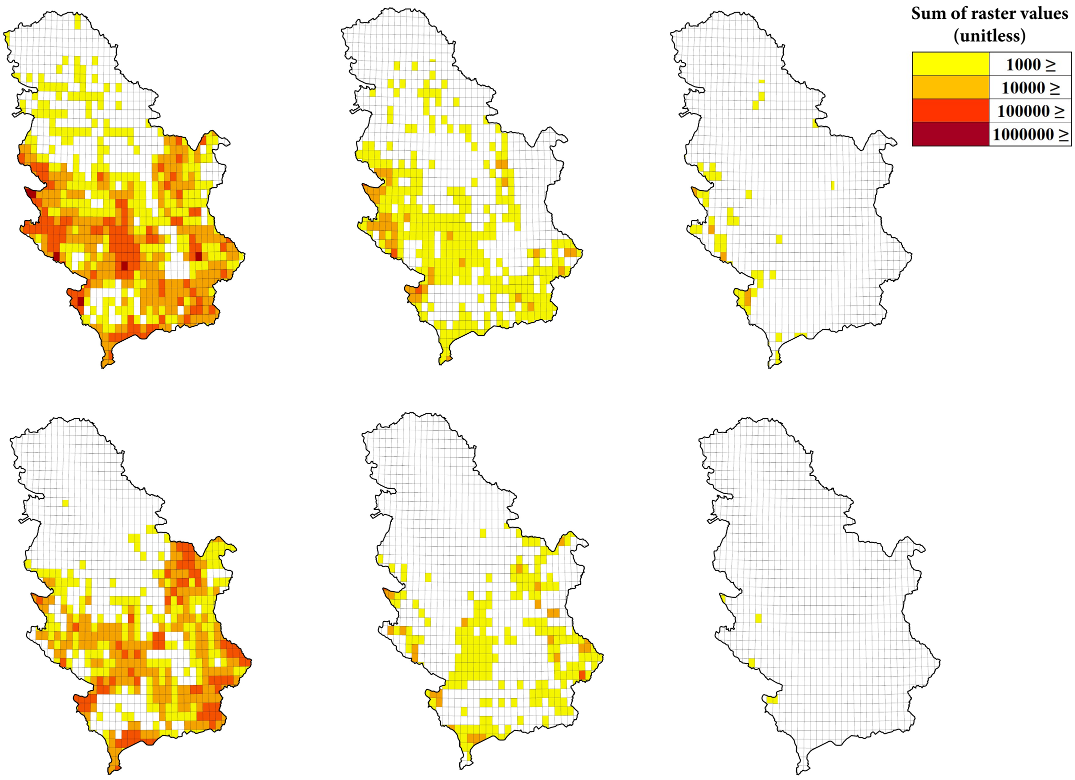


*(ascending: a–c layover, shadow, combined; descending: d–f layover, shadow, combined) (created by author).*

Comparing the two approaches, the mean-based statistics effectively describe the average intensity and spatial distribution of distortions, highlighting where distortions are consistently present, whereas the sum-based analysis emphasizes cumulative distortion hotspots and repeated overlapping effects across multiple scenes. Together, these complementary metrics confirm that western and central Serbia, along with selected southern and eastern regions, are most susceptible to persistent radar distortions, with ascending acquisitions generally producing more extensive spatial coverage, while descending acquisitions concentrate distortions in specific areas. This combined interpretation underscores the importance of considering both the statistical method and acquisition geometry when evaluating SAR imagery quality and planning subsequent interferometric or geodetic analyses.

### 4.2. PRACTICAL IMPLICATIONS FOR CORNER REFLECTOR DEPLOYMENT

The analysis of terrain-induced distortions and radar shadowing patterns presented in this study provides critical insights for the practical deployment of passive corner reflectors (CR). While previous sections highlighted the general advantages of having accurate distortion maps, the findings here allow for a more nuanced application in site selection for reflectors.

One of the key practical criteria for the effective deployment of a network of corner reflectors is the identification and avoidance of regions prone to radar shadowing or layover effects. Areas that consistently experience such distortions can significantly compromise the quality of radar backscatter measurements, reducing the reliability of subsequent SAR analyses. By integrating distortion maps into the planning process, potential deployment sites can be evaluated not only for accessibility and land use constraints but also for their radar visibility.

In this context, the present work demonstrates a methodology for discriminating suitable areas based on their radar response characteristics. This approach can guide future efforts in establishing permanent or temporary reflector networks, ensuring that each deployed reflector maximizes its signal visibility and contributes to the overall calibration or monitoring objectives. Furthermore, these results can inform the design of deployment strategies that prioritize regions with minimal distortion while accounting for the spatial distribution necessary for calibration.

While the present study does not implement an optimization algorithm for reflector placement, the generated distortion layers represent a necessary first-order constraint in any future multi-criteria site selection framework.

## 5. CONCLUSION

This study provides the first systematic and quantitative analysis of the spatial distribution of geometric distortions in Sentinel-1 SAR imagery over the territory of the Republic of Serbia. By combining a precisely defined processing workflow, including SAR simulation, terrain correction, and advanced GIS-based spatial analysis, a unique dataset was generated that cartographically and statistically describes the occurrence of layover, radar shadow, and their combined effects under different orbital configurations.

The results clearly indicate pronounced spatial heterogeneity of distortions, as well as a strong dependence of their intensity and spatial distribution on terrain characteristics and acquisition geometry. The identified differences between ascending and descending orbits further confirm that the interpretation of Sentinel-1 data must be conditioned by orbital parameters, particularly in areas characterized by complex topography. Through the use of complementary statistical metrics (mean and sum), it was possible to simultaneously assess average distortion intensity and cumulative spatial concentration, resulting in a more robust interpretation of radar signal degradation patterns.

One of the key contributions of this work is the creation of a publicly available, nationally comprehensive spatial dataset of geometric distortions. The open availability of the dataset further enhances its long-term usability by enabling integration with other geospatial data sources and application across a wide range of thematic domains, including geodynamics, infrastructure monitoring, natural hazard assessment, and spatial planning.

Beyond its immediate scientific contributions, the results of this study also demonstrate significant practical value. The generated spatial distortion maps can be used as a primary filtering layer in the planning of interferometric analyses, the selection of stable reference areas, and the assessment of radar measurement reliability in complex terrain. In this context, the produced dataset represents a fundamental knowledge infrastructure that supports informed decision-making in subsequent phases of SAR-based research and operational applications.

The results of this research also represent one of the determining criteria in the future development of a national network of corner reflectors in Serbia. The spatial distribution of geometric distortions defines fundamental constraints on radar visibility and directly affects the reliability of reflector backscatter responses. By integrating the generated distortion maps into the planning process, it becomes possible to identify locations characterized by stable acquisition geometry and minimal influence of layover and radar shadow, thereby ensuring optimal conditions for long-term SAR and InSAR measurements. In this way, the present work not only contributes to a better understanding of the spatial structure of SAR limitations, but also establishes an objective, quantitative basis for reflector site selection within the broader research framework focused on the development of reference radar infrastructure in the Republic of Serbia.

**LITERATURE**


[1] I. H. Woodhouse, *Introduction to Microwave Remote Sensing*, 1st ed. Boca Raton, FL, USA: CRC Press, 2006, pp. 390–410, doi: 10.1201/9781315272573.

[2] D. Pairman and S. McNeill, "Efficient calculation in the map domain of SAR layover and shadow masks," in *Proc. IGARSS '97 – IEEE Int. Geosci. Remote Sens. Symp.*, Singapore, 1997, vol. 4, pp. 2057–2059, doi: 10.1109/IGARSS.1997.609220.

[3] J. C. Curlander and R. N. McDonough, *Synthetic Aperture Radar: Systems and Signal Processing*. New York, NY, USA: Wiley, 1991.

[4] R. Yun, Z. Huanxin, Z. Shilin, S. Hao, and J. Kefeng, "A method to detect layover and shadow based on distributed spaceborne single-baseline InSAR," *IOP Conf. Ser.: Earth Environ. Sci.*, vol. 17, no. 1, 2014, doi: 10.1088/1755-1315/17/1/012235.

[5] U. Stilla, U. Soergel, and U. Thoennessen, "Potential and limits of InSAR data for building reconstruction in built-up areas," *ISPRS J. Photogramm. Remote Sens.*, vol. 58, nos. 1–2, pp. 113–123, Jun. 2003.

[6] C. Shi, X. Zuo, J. Zhang, D. Zhu, Y. Li, and J. Bu, "Accuracy assessment of geometric-distortion identification methods for Sentinel-1 synthetic aperture radar imagery in highland mountainous regions," *Sensors*, vol. 24, no. 9, 2024, doi: 10.3390/s24092834.

[7] W. G. Kropatsch and D. Strobl, "The generation of SAR layover and shadow maps from digital elevation models," *IEEE Trans. Geosci. Remote Sens.*, vol. 28, no. 1, pp. 98–107, 1990, doi: 10.1109/36.45752.

[8] A. J. Wilkinson, "Synthetic aperture radar interferometry: A model for the joint statistics in layover areas," in *Proc. South African Symp. Commun. Signal Process. (COMSIG '98)*, 1998, pp. 333–338.

[9] S. Plank, J. Singer, C. Minet, and K. Thuro, "GIS-based suitability evaluation of the differential radar interferometry method (D-InSAR) for detection and deformation monitoring of landslides," in *Proc. FRINGE 2009*, Frascati, Italy, 2009.

[10] X. Liu, Y. Song, and R. Yang, "Layover solution based on unitary ESPRIT algorithm in multi-baseline InSAR," *J. Electron. Inf. Technol.*, vol. 30, no. 7, pp. 1525–1528, 2008.

[11] Y. Tian, C. Ding, M. Shi, and F. Zhang, "Layover detection using neural network based on expert knowledge," *Remote Sens.*, vol. 14, no. 23, 2022, doi: 10.3390/rs14236087.

[12] X. Cai et al., "Automatic extraction of layover from InSAR imagery based on multilayer feature fusion attention mechanism," *IEEE Geosci. Remote Sens. Lett.*, vol. 19, pp. 1–5, 2022.

[13] A. Tiwari, A. B. Narayan, and O. Dikshit, "Deep learning networks for selection of measurement pixels in multi-temporal SAR interferometric processing," *ISPRS J. Photogramm. Remote Sens.*, vol. 166, pp. 169–182, Aug. 2020.

[14] X. Li, G. Zhang, C. Yin, Y. Wu, and X. Shen, "A novel shadow and layover segmentation network for multi-angle SAR images fusion," *IEEE Access*, vol. 10, pp. 117770–117781, 2022, doi: 10.1109/ACCESS.2022.3217510.

[15] F. Cigna, L. B. Bateson, C. J. Jordan, and C. Dashwood, "Simulating SAR geometric distortions and predicting persistent scatterer densities for ERS-1/2 and ENVISAT C-band SAR and InSAR applications," *Remote Sens. Environ.*, vol. 152, pp. 441–466, 2014, doi: 10.1016/j.rse.2014.06.025.

[16] X. Chen, Q. Sun, and J. Hu, "Generation of complete SAR geometric distortion maps based on DEM and neighbor gradient algorithm," *Appl. Sci.*, vol. 10, no. 11, 2018, doi: 10.3390/app8112206.

[17] M. Basarić, "Comparative analysis of Sentinel-1 InSAR ground motion data dissemination strategies: Towards an optimal model for Serbia," *Int. Arch. Photogramm. Remote Sens. Spatial Inf. Sci.*, vol. XLVIII-4/W13-2025, pp. 57–64, 2025, doi: 10.5194/isprs-archives-XLVIII-4-W13-2025-57-2025.

[18] H. Peter et al., "Sentinel-1A – First precise orbit determination results," *Adv. Space Res.*, vol. 60, no. 5, pp. 879–892, 2017, doi: 10.1016/j.asr.2017.05.034.

[19] H. Peter, J. Fernández, and P. Féménias, "Copernicus Sentinel-1 satellites: Sensitivity of antenna offset estimation to orbit and observation modelling," *Adv. Geosci.*, vol. 50, pp. 87–100, 2020, doi: 10.5194/adgeo-50-87-2020.

[20] DIVA-GIS, Administrative Areas (Boundaries). Accessed: Dec. 2025. [Online]. Available: https://diva-gis.org/data.html

[21] Alaska Satellite Facility, ASF Search, Geophysical Institute, University of Alaska Fairbanks. Accessed: Dec. 2025. [Online]. Available: https://search.asf.alaska.edu/

[22] European Space Agency (ESA). (2014). *Sentinel-1 SAR IW SLC dataset, ascending and descending orbits, 21 images over Serbia (november, 2025)* [Satellite imagery]. Copernicus Open Access Hub. https://scihub.copernicus.eu/

[23] National Aeronautics and Space Administration – NASA (2000) Shuttle Radar Topography Mission (SRTM) Data.[Dataset]. United States Geological Survey (USGS) Earth Explorer. Available at: https://earthexplorer.usgs.gov/

[24] T. G. Farr et al., "The Shuttle Radar Topography Mission," *Rev. Geophys.*, vol. 45, no. 2, 2007, Art. no. RG2004, doi: 10.1029/2005RG000183.

[25] European Space Agency (ESA). SNAP – ESA Sentinel Application Platform (Version 13.0.0) [Software], Science Toolbox Exploitation Platform (STEP), 2025. [Online]. Available: http://step.esa.int/main/download/snap-download/

[26] Esri. (2023). ArcGIS Pro (Version 3.01) [Software]. Redlands, CA, USA: Environmental Systems Research Institute. Accessed: 16 December 2025. [Online]. Available: https://www.esri.com/en-us/arcgis/products/ arcgis-pro/overview

[27] "SAR Simulation Operator," SNAP Science Toolbox Exploitation Platform (STEP), Version 9.0.0, European Space Agency, Accessed: Dec. 2025. [Online]. Available: https://step.esa.int/main/wp-content/help/versions/9.0.0/snaptoolboxes/org.esa.s1tbx.s1tbx.op.sar.processing.ui/operators/SARSimulationOp.html

[28] "SAR Simulation Terrain Correction Operator," SNAP Science Toolbox Exploitation Platform (STEP), Version 9.0.0, European Space Agency, Accessed: Dec. 2025. [Online]. Available: https://step.esa.int/main/wp-content/help/versions/9.0.0/snap-toolboxes/org.esa.s1tbx.s1tbx.op.sar.processing.ui/operators/SARSimTerrainCorrectionOp.html

[29] H. Liu, Z. Zhao, and K. C. Lezek, "Correction of positional errors and geometric distortions in topographic maps and DEMs using a rigorous SAR simulation technique," *Photogramm. Eng. Remote Sens.*, vol. 70, no. 9, 2004.

[30] G. Schreier, *SAR Geocoding: Data and Systems*. Karlsruhe, Germany: Wichmann-Verlag, 1993, pp. 173–180.

[31] Esri, "How zonal statistics tools work, ArcGIS Pro | Documentation," ArcGIS Pro Documentation. Accessed: Jan. 10, 2026. [Online]. Available: https://pro.arcgis.com/en/pro-app/latest/tool-reference/spatial-analyst/how-zonal-statistics-works.htm

[32] Esri, "Zonal Statistics (Spatial Analyst), ArcGIS Pro | Documentation," ArcGIS Pro Documentation. Accessed: Jan. 10, 2026. [Online]. Available: https://pro.arcgis.com/en/pro-app/3.5/tool-reference/spatial-analyst/zonal-statistics.htm

[33] Esri. (2015). "Topographic" [basemap]. Scale Not Given. "World Hillshade". Accessed: Jan. 9, 2026. [Online]. Available: https://www.arcgis.com/home/item.html?id= 1b243539f4514b6ba35e7d995890db1d